9
Nanoscale Localized Surface Plasmon Resonance Biosensors

Katherine A. Willets, W. Paige Hall, Leif J. Sherry, Xiaoyu Zhang, Jing Zhao, and Richard P. Van Duyne

9.1
Overview

The interaction of light with metallic nanoparticles (NPs) has aroused significant interest in recent years due to demonstrated applications in nanoscale lithography [1–3], surface-enhanced spectroscopies [4–9], and chemical and biological sensing applications [10–14]. In each of these examples, light can be localized, manipulated, and amplified on the nanometer scale by exciting a collective electron oscillation in the metallic NPs, known as localized surface plasmon resonance (LSPR). By controlling the size, shape, material and local dielectric environment of the NPs, the resonance condition of the plasmon can be tuned throughout the visible and near-infra-red (IR) ranges [15–21]. It is the latter property – namely the local dielectric environment – which forms the basis of LSPR-based biosensing experiments [10, 11, 14, 22–28].

Before discussing LSPR and its applications in detail, the basic physics of plasmons will be briefly reviewed [20]. When a metal surface (either bulk or nanoscale) is irradiated with electromagnetic radiation (light) of the appropriate frequency, a coherent oscillation of the metal's conduction electrons is induced orthogonal to the propagation direction of the light. This oscillation is a ''plasmon'', and it can be analyzed as fluctuations in the metal's surface electron density or, in other words, as a longitudinal electron density wave. In the case of metallic NPs with sizes less than the wavelength of the incident radiation, this plasmon is localized on the surface of the NP (in contrast to bulk metal, where the plasmon can propagate along the surface plane and evanescently decay perpendicular to the plane). This principle is illustrated in Figure 9.1, where the electron cloud of a metallic NP oscillates in phase with the incident electromagnetic field.

The wavelength at which this resonance occurs depends on a number of factors related to both the NP itself, as well as its local environment. Typically, gold and silver NPs are chosen for most LSPR applications, although other metals such as

Nanobiotechnology II. Edited by Chad A. Mirkin and Christof M. Niemeyer

ISBN: 978-3-527-31673-1

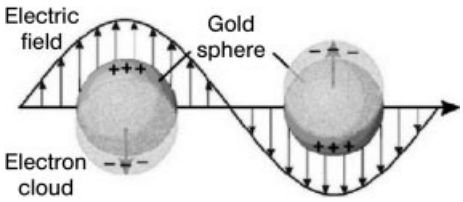

Fig. 9.1 Illustration of the oscillation of conduction band electrons of a gold nanoparticle with an electromagnetic field, resulting in a localized surface plasmon.

aluminum and copper can also support plasmons [29, 30]. The size and shape of these NPs also dictates the resonance condition; for example, a silver cube will have a plasmon resonance red shifted relative to a silver sphere of the same volume [7]. Lastly, the plasmon resonance is affected by the local environment of the NP – either through the bulk (solvent) refractive index or through the adsorption of some species to the NP surface [24, 25, 31–33]. By understanding the contributions from each of these factors, it should be possible to design better LSPR sensors for biosensing applications.

In order to provide a more quantitative description of the relationships described above, Mie theory – which models the extinction of a single sphere of arbitrary material – is often used [34]. Mie theory analytically solves Maxwell's equations with appropriate boundary conditions in spherical coordinates. In the dipole limit, where the dimension of the sphere is much smaller than the incident wavelength ($a \ll \lambda$), the extinction cross-section, $\mathrm{E}(\lambda)$, of a sphere can be estimated by the following equation:

$$\mathrm{E}(\lambda) = \frac{24\pi^2 a^3 \varepsilon_m^{3/2}}{\lambda \ln(10)} \left[\frac{\varepsilon_i}{(\varepsilon_r + 2\varepsilon_m)^2 + \varepsilon_i^2} \right] \tag{1}$$

where a is the radius of the sphere, ε_m is the dielectric constant of the medium surrounding the sphere, λ is the wavelength of the absorbing radiation, and ε_r, ε_i are the real and imaginary portions of the sphere's dielectric function, respectively. From this primitive estimation, it can be seen that the extinction of a single sphere depends on its size (a), material ($\varepsilon_r, \varepsilon_i$), and the surrounding environment (ε_m). For non-spherical particles of arbitrary shape, the extinction cross-section also depends on their geometry, and this can be modeled by substituting the term $\chi\varepsilon_m$ for $2\varepsilon_m$ in Eq. (1), where χ contains information about the shape and aspect ratio of a particle of arbitrary geometry [21]. Typically, for these more complicated structures, numerical methods to solve Maxwell's equation are used in order to model the optical properties of objects with arbitrary shapes in various dielectric environments [20]. Two of the most commonly used numerical methods are the discrete dipole approximation (DDA), and the finite-difference time-domain (FDTD) method [35, 36]. In these two approaches, the particle of interest

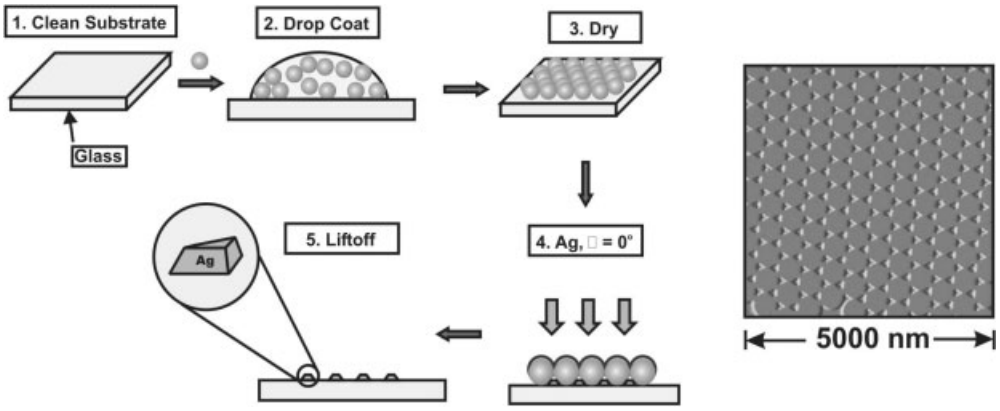

Fig. 9.2 Left: Nanosphere lithographic fabrication of nanoparticle arrays. Right: Atomic force microgram of nanoparticle array fabricated with nanosphere lithography.

is divided into finite elements. In the DDA method, Maxwell's equations are solved in the frequency domain, whereas in the FDTD method they are solved in the time domain. Using these two numerical methods on NPs of various shapes and sizes leads to different predicted resonances.

Because different shapes can tune the LSPR resonance, a great deal of effort has been focused on producing NPs of different geometries. In fact, a large number of protocols has been published for synthesizing both Au and Ag NPs using various methods, often in the presence of stabilizing surfactants [18, 37–43]; as these syntheses become more refined, particles with well-defined shapes and narrow size distributions can be produced. Lithographic techniques, such as electron-beam [44] or nanosphere lithography (NSL) [19], have also been employed in the fabrication of NPs, especially for large-scale arrays. Figure 9.2 (right panel) shows an example of an array of nanoscale triangles produced using NSL. In NSL, a hexagonally close-packed array of polymer spheres is used as a mask through which metal can be deposited (see Figure 9.2). For sensing experiments, such NP arrays are often preferred because they allow a large surface area to be interrogated using a commercially available UV-visible spectrometer; however, single NP LSPR spectroscopy is also possible and can offer zeptomole sensitivity [11].

In addition to designing NPs with specific LSPR resonances, as described above, it is also important for the NPs to provide a large response to changes in their local environment. This response can be modeled using Eq. (2), which relates the shift in the maximum wavelength of the LSPR resonance ($\Delta\lambda_{\max}$) to the presence of an adsorbed species [45]:

$$\Delta\lambda_{\max} = m\Delta n\left[1 - \exp\left(\frac{-2d}{l_d}\right)\right] \tag{2}$$

Here, m is the refractive index response of the NPs, Δn is the change in refractive index induced by the adsorbate, d is the effective adsorbate layer thickness, and l_d is the characteristic electromagnetic field decay length (approximated as an exponential decay). The ability to sense the binding of an adsorbate to the NP surface through a shift in the LSPR resonance is the key principle behind most biosensing experiments, and thus it is critical to design NP systems that offer both large refractive index responses (m) and short-range electromagnetic field enhancements (small l_d). It is this latter term that provides the biggest advantage in using LSPR versus traditional SPR techniques [28], due to the fact that fields can be highly localized and confined to small volumes around the NPs.

The remainder of this chapter will focus on methods related to LSPR spectroscopy for biosensing. Initially, the different NP geometries for both array and single particle LSPR experiments are discussed, emphasizing the LSPR response to changes in the local environment. Subsequently, an example in which LSPR spectroscopy has been applied to biosensing – specifically, the detection of an Alzheimer's disease biomarker – will also be provided. Finally, the outlook for LSPR spectroscopy for biosensing will be examined.

9.2 Methods

9.2.1 Nanofabrication of Materials for LSPR Spectroscopy and Sensing

As described above, there are a number of factors that determine the LSPR properties of metallic NPs; hence, choosing the correct NP system for biosensing requires an understanding of how NPs of different morphologies respond to controlled changes in their local environment. This is typically characterized by the refractive index sensitivity, m [see Eq. (2)], although a new figure of merit (FOM) has recently been introduced to describe the performance of single NPs as sensors of environmental change [46].

$$FOM = \frac{m(eV\ RIU^{-1})}{FWHM(eV)} \tag{3}$$

By normalizing m to the full-width-half-maximum (FWHM) of the spectral peak, NPs of different shapes and sizes can be directly compared.

Recent studies have highlighted several new strategies and techniques for improvements in the fabrication and characterization of both NP arrays and single NPs for LSPR. For example, the NSL-fabricated triangles described above can be electrochemically oxidized to tune both their size and shape on a length scale ranging from ~1 nm to several tens of nanometers [47]. The particular power of this approach is that the triangles are preferentially oxidized: first at the bottom

edges, then at the triangular tips, and finally from the top face, allowing the response of LSPR to changes in morphology to be directly correlated. Alternatively, a novel technique known as atomic layer deposition (ALD) is available for determining the precise distance-dependence of the local field enhancement [i.e., l_d in Eq. (2)] [48]. Atomic layers of Al_2O_3 are deposited on NSL-fabricated arrays, and the shift in the LSPR spectrum is measured as a function of film thickness. Finally, electron beam lithography is available to determine the effect of diffractive coupling on the peak position and linewidth of LSPR spectra. By fabricating one-dimensional (1-D) cylindrical arrays with various interparticle spacing, this coupling can be observed through the emergence of a narrow feature in the extinction spectrum [49]. Because each of these techniques offers precision control over NP structure and local environment, parameters affecting the plasmon resonance can be studied in detail.

Beyond using new methods to better understand the relationships between particle shape, local environment, coupling and the LSPR spectrum, it is also important to develop new LSPR materials for use in biosensing experiments. While this has been a field of active research, with new geometries frequently reported, here we describe three recent systems that have been characterized in detail. In particular, the LSPR response of these systems to changes in the local environment – whether through a bulk refractive index change or interparticle coupling – are described for each system.

9.2.1.1 Film Over Nanowells

Nanohole or nanowell arrays have recently begun to be analyzed as a new plasmonic construct since the discovery of enhanced transmission through subwavelength apertures [50–52]. Nanowell structures have been successfully fabricated using reactive ion etching (RIE) through a polystyrene mask (in analogy to the mask used for NSL), followed by thermal vapor deposition of a 50-nm silver film (Figure 9.3) [53]. The thickness of the Ag film (d_m) was selected to be at least 50 nm to allow for efficient reflectance from the surface. When substrates are not optically transparent, the wavelength associated with minimum reflectivity (λ_{min}) provides an alternative measure of the LSPR λ_{max}. This study has revealed that

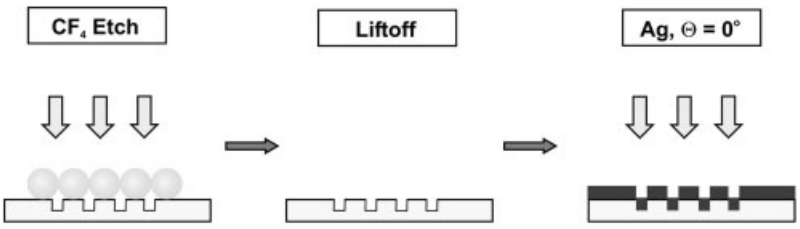

Fig. 9.3 Schematic illustration of the preparation of the film over nanowell surfaces, starting from a sphere mask as shown in Figure 9.2 (steps 1–3).

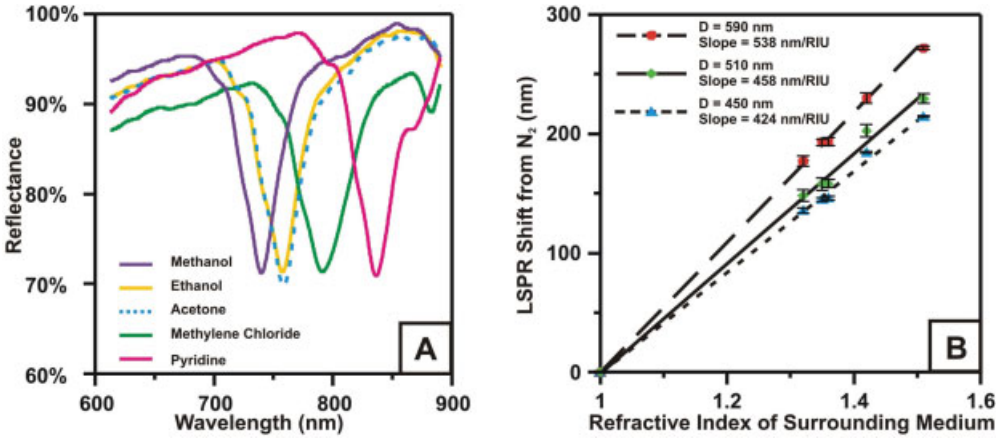

Fig. 9.4 (A) A collection of reflectance spectra of an Ag film over nanowell surface in different solvents (D = 590 nm, d_m = 50 nm). (B) Plots of the [λ_{min}(solvent) − λ_{min}(dry nitrogen)] versus refractive index of the solvent for three nanosphere sizes: D = 450, 510, and 590 nm. Each datum point represents the average value obtained from at least three surfaces; error bars show standard deviations. For all surface preparations, d_m = 50 nm and etching time t_e = 10 min. (Reproduced with permission from Ref. [53]; © 2005 American Chemical Society.)

these nanowells have both extremely narrow plasmon resonances and very strong wavelength sensitivity to the external dielectric constant (∼500 nm RIU^{-1}) [53]. The effect of external dielectric media on the plasmon peak was studied by altering the surrounding solvent and monitoring the LSPR changes (see Figure 9.4A) [53]. Figure 9.4B shows plots of [λ_{min}(solvent) − $\lambda_{min}(N_2)$] for film over nanowell substrates as a function of the refractive index of the surrounding medium [53]. Within this range of refractive index units (RIU), the data points for the surfaces fabricated using the same size polystyrene nanosphere can be fitted well to a linear regression. It is found that the film over nanowell surface using the largest sphere (D = 590 nm) is the most sensitive to changes in the surrounding refractive index, followed by D = 510 nm, then D = 450 nm. For the most sensitive film over nanowell surfaces (D = 590 nm), the linear regression analysis yielded a refractive index sensitivity [i.e., m from Eq. (2)] of 538 nm RIU^{-1}; this means that every change of 0.002 in the refractive index of the solvent will produce a change in the peak position of approximately 1 nm.

9.2.1.2 Solution-Phase NSL-Fabricated Nanotriangles

A novel technique has recently been reported to produce monodisperse solution-phase NPs by releasing NSL-fabricated surface-confined NPs into solution [54]. The fabrication procedure is illustrated schematically in Figure 9.5 (upper panel). Surface-bound NSL-fabricated NPs are incubated in an alkanethiol solution to form a self-assembled monolayer (SAM) on the NPs (steps 1 and 2). Following

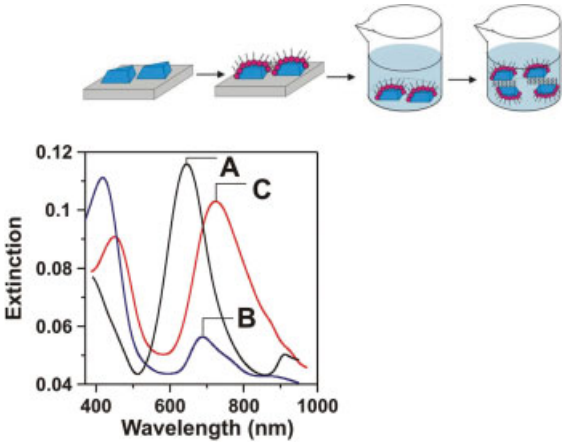

Fig. 9.5 Upper: Schematic illustration of the procedure for releasing NSL-fabricated triangles into solution. Lower: UV-visible extinction spectra of (A) surface-bound, (B) monomeric solution-phase, and (C) dimeric solution phase SAM-functionalized, NSL-fabricated Ag nanoparticles in ethanol. (Reproduced with permission from Ref. [54]; © 2005 American Chemical Society.)

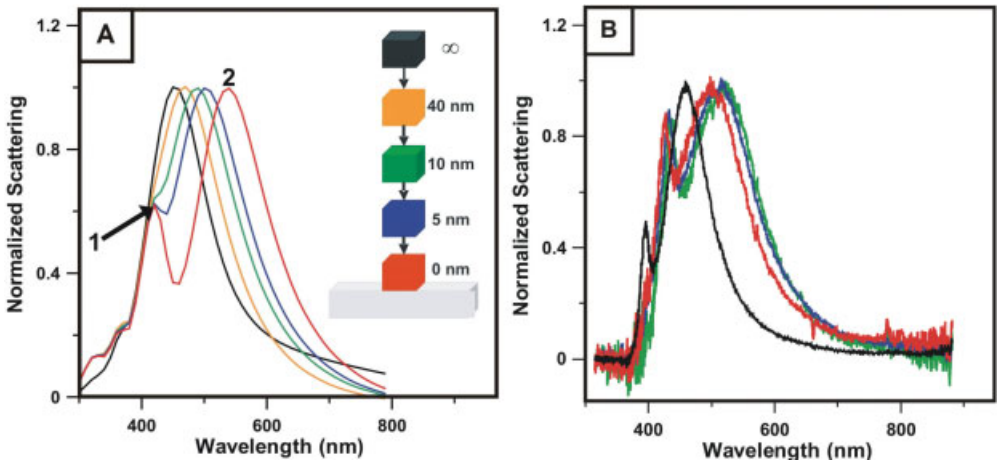

Fig. 9.6 (A) Finite-difference time-domain theory showing the emergence of a second peak as a single nanocube (90 nm diameter) approaches a dielectric substrate. (B) Refractive index sensitivity demonstrated by dark-field scattering spectra in four different dielectric environments [refractive indices: 1.000297 (black); 1.329 (red); 1.3854 (blue); 1.4458 (green)]. (Reproduced with permission from Ref. [46]; © 2005 American Chemical Society.)

SAM functionalization, the Ag NPs are released into solution by sonication in ethanol (step 3). During the releasing process described above, all sides of the released NPs are coated with SAM, except for the bases of the triangles, which were in contact with the glass substrate; this allows the NPs to be asymmetrically functionalized. For example, a dithiol linking agent can be added to the NP solution in order to functionalize the bases, leading to linked NP dimers (step 4). The formation of solution-phase NP monomers and dimers has been verified using transmission electron microscopy (TEM) [54].

The optical properties of the surface-bound and solution-phase SAM-functionalized Ag NPs have been characterized using UV-visible extinction spectroscopy, as shown in Figure 9.5 (lower panel). The spectrum of the released NPs (spectrum B) differs dramatically from that of the particle array on the glass substrate (spectrum A). Two peaks appear in the released NP spectrum – an intense peak at 418 nm and a weak, broad peak centered at 682 nm. Upon forming the linked NP dimers, a further change in the UV-visible spectrum of the NP solution is observed (spectrum C): the high-energy peak shifts from 418 nm to 431 nm and decreases in intensity, while the low-energy peak at 682 nm shifts to 705 nm and increases in intensity and peak width. These observations have been explained using the DDA method, which describes both the origin of the two peaks as well as the shifts upon dimerization [54]. The ability to asymmetrically functionalize these solution-phase NPs to induce formation of specific targets – such as NP dimers – is a significant advantage in certain LSPR biosensing experiments, and will be pursued in future applications.

9.2.1.3 **Silver Nanocubes**

Silver nanocubes prepared by the polyol synthesis [55, 56] offer a unique plasmonic response when single-particle LSPR spectra are measured on a glass substrate; namely, there are *two* plasmon resonance peaks (as in Figure 9.6) [46]. This is because the dielectric symmetry of their environment is broken when they are placed on a glass substrate. For a NP to yield a new plasmon resonance peak when it is placed on a dielectric surface, it must satisfy two conditions: (i) its near fields must be most intense at the polar regions of the NP; and (ii) it must be thicker than the skin depth of the material (~25 nm for silver) [46].

In order to understand the physical origin of these peaks, FDTD calculations were performed to model the near-field behavior of the cubes [46]. Figure 9.6A shows a series of scattering spectra that were generated from calculations in which the cube is moved progressively closer to a dielectric surface. These spectra show that the dipole mode associated with the solution spectrum shifts into a broad peak at 550 nm when the particle closes to within a few nanometers of the surface. In addition, a blue peak appears at 430 nm that becomes more distinct as the particle approaches the surface. Figure 9.6B shows experimental data from a single nanocube in which a change in the local refractive index is accompanied by a shift in the plasmon resonance of both the high- and low-energy peaks. In particular, the response of the higher energy peak to the change in refractive index proves to be more sensitive than the standard dipole resonances of other NPs

due to the narrow linewidth of this peak – that is, the FOM value is 5.4 [46]. This suggests that these particles may offer an advantage over other NP geometries for sensing experiments.

9.2.2 Biosensing

Each of the NP geometries described above – as well as many other NP platforms – can be used for biosensing experiments in which the binding of a biological target can induce a measurable shift in the LSPR spectrum. By appropriately functionalizing NP surfaces, LSPR sensors can be designed to detect a variety of biological and pathogenic molecules, making them a valuable diagnostic tool for the biomedical industry. The sensitivity of LSPR sensors for a number of biologically relevant systems has already been demonstrated [14, 23, 26–28, 57, 58]. In this section, we will describe one of the most important biological applications of the LSPR sensor to date, namely the detection and diagnosis of a possible biomarker for Alzheimer's disease [26, 27].

One hallmark of Alzheimer's disease is the formation of insoluble protein deposits, known as amyloid plaques, in brain tissue. These plaques are formed from the soluble precursor amyloid beta, a small 39- to 43-amino acid protein that is present in elevated levels in the brain and cerebral spinal fluid (CSF) of Alzheimer's disease sufferers [59]. Single units of amyloid beta readily assemble into oligomers of two to 24 units (sometimes referred to as amyloid-β-diffusible ligands, or ADDLs), and these oligomers themselves exhibit significant neuronal toxicity [60]. Though not proven, it is increasingly likely that ADDLs may cause early memory loss in Alzheimer's disease [61, 62]. Currently, the diagnosis of Alzheimer's disease is made based on symptomatic evidence, there being no diagnostic method based on the molecular pathology of the disease currently available.

The LSPR sensor, however, represents a promising step towards the molecular detection of the ADDL biomarker. Antibodies which specifically recognize amyloid beta oligomers [63] were covalently attached to a chemical monolayer on an NSL-fabricated NP surface (Figure 9.7A; step 1). Subsequently, CSF from patients diagnosed with Alzheimer's disease or from healthy, age-matched controls was flowed over the sensor surface (step 2). Any amyloid beta oligomers that remained bound to the antibody-functionalized surface were detected using a second capping antibody (step 3), thus completing the ''sandwich'' assay. By measuring extinction shifts in response to the addition of capping antibody, it was shown that diseased patients (Figure 9.7C) had significantly higher concentrations of amyloid beta oligomers than did age-matched controls (Figure 9.7B) [27]. The experiment was repeated using soluble post-mortem brain extract from diseased and control patients, with similar results [27].

The results from this study not only confirmed the relationship between elevated amyloid beta levels and Alzheimer's disease, but also suggested that the LSPR sensor could be used as an early detection technique for the condition. Moreover, the sandwich assay described above is broadly generalizable, suggesting that the LSPR sensors might have applications for other biosensing applications.

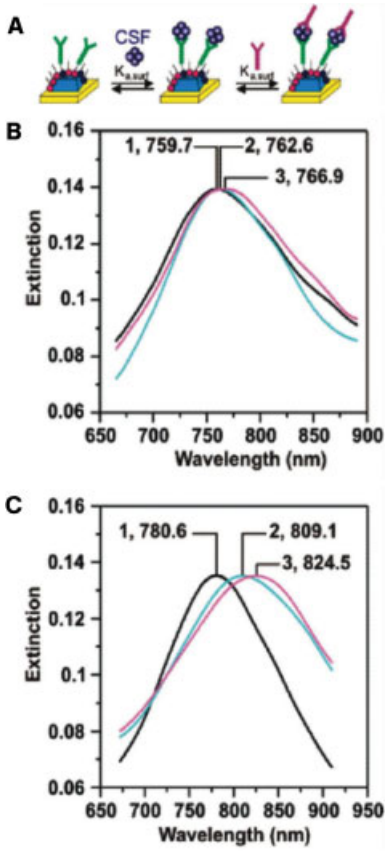

Fig. 9.7 (A) Schematic showing the localized surface plasmon resonance (LSPR) sandwich assay. Antibodies are linked to a SAM-covered nanoparticle (step 1). Amyloid-β-diffusible ligands (ADDLs) are then introduced that bind to the antibodies (step 2). Finally, a second capture antibody binds (step 3), completing the sandwich. (B) LSPR spectra for each step of the assay for an aging patient: (B-1) 100 nM anti-ADDL (λ_{max} = 759.7 nm); (B-2) CSF (λ_{max} = 762.6 nm); and (B-3) 100 nm anti-ADDL (λ_{max} = 766.9 nm). (C) LSPR spectra for each step of the assay for an Alzheimer's patient: (C-1) 100 nm anti-ADDL (λ_{max} = 780.6 nm); (C-2) CSF (λ_{max} = 809.1 nm); and (C-3) 100 nm anti-ADDL (λ_{max} = 824.5 nm). All measurements were made in a nitrogen environment. (Reproduced with permission from Ref. [27]; © 2005 American Chemical Society.)

9.3 Outlook

In this chapter, we have described methods related to the fabrication, characterization, and use of NPs for LSPR biosensing experiments. By using novel techniques such as electrochemistry, atomic layer deposition, and electron-beam lithography of 1-D arrays, the properties of these NP systems can be explored

in a controlled manner. Moreover, several architectures for LSPR substrates – including nanowells, released NSL-fabricated nanotriangles and nanocubes – have been described in detail, with a particular emphasis on their ability to sense changes in their local environment. Finally, a sensor for the detection of a biomarker for Alzheimer's disease has been demonstrated using human samples.

In comparison to traditional propagating surface plasmon resonance (SPR) spectroscopy at smooth, thin metal film surfaces, LSPR has been shown to offer comparable speed and sensitivity [28]. However, unlike SPR, LSPR spectroscopy allows very small distances to be probed due to the decay in the electromagnetic field enhancement as one moves away from the NP surface. Moreover, SPR is an inherently ''bulk'' technique, whereas LSPR spectra can be measured for individual NPs, which may offer improvements in both speed and sensitivity. Several strategies are available to achieve such improvements for both the array and single particle formats. In particular, new NP geometries continue to be explored, with an eye towards narrower LSPR linewidths and better control over lineshapes. Moreover, the development of new amplification strategies in order to maximize the wavelength shift upon analyte binding should reduce the limit of detection into concentration regimes currently inaccessible with this technique. Such strategies include the introduction of secondary labels – such as NPs, enzymes or even resonant molecules – to the binding assays in order to maximize the wavelength shift. Lastly, single-particle LSPR is a promising approach, despite current limitations which mean that the spectra cannot be measured rapidly and in parallel. However, new wavelength-scanning liquid crystal tunable filters may help to overcome this issue. Thus, LSPR promises to remain competitive as a technique for biological sensing applications.

Acknowledgments

The authors gratefully acknowledge support from the Air Force Office of Scientific Research MURI program (grant F49620-02-1-0381), the National Science Foundation (EEC-0118025, DMR-0076097, CHE-0414554, DMR-0520513, BES-0507036), and the National Cancer Institute (1 U54 CA119341-01).

References

1 Srituravanich, W., Fang, N., Sun, C., Luo, Q., Zhang, X. (2004) Plasmonic nanolithography. *Nano Lett.* **4**, 1085–1088.

2 Sundaramurthy, A., Schuck, P. J., Conley, N. R., Fromm, D. P., Kino, G. S., Moerner, W. E. (2006) Toward nanometer-scale optical photolithography: utilizing the near-field of bowtie optical nanoantennas. *Nano Lett.* **6**, 355–360.

3 Kik, P. G., Maier, S. A., Atwater, H. A. (2004) Surface plasmons for nanofabrication. *Proc. SPIE-Int. Soc. Opt. Eng.* **5347**, 215–223.

4 Schatz, G. C., Van Duyne, R. P. (2002) In: Chalmers, J. M., Griffiths, P. R. (Eds.), *Handbook of Vibrational*

Spectroscopy. Wiley, New York, Vol. 1, pp. 759–774.

5 Haynes, C. L., Van Duyne, R. P. (2003) Plasmon-sampled surface-enhanced Raman excitation spectroscopy. *J. Phys. Chem. B* **107**, 7426–7433.

6 Emory, S. R., Nie, S. (1997) Probing single molecules and single nanoparticles by surface-enhanced Raman scattering. *Science* **275**, 1102–1106.

7 Haes, A. J., Haynes, C. L., McFarland, A. D., Zou, S., Schatz, G. C., Van Duyne, R. P. (2005) Plasmonic materials for surface-enhanced sensing and spectroscopy. *MRS Bull.* **30**, 368–375.

8 McFarland, A. D., Young, M. A., Dieringer, J. A., Van Duyne, R. P. (2005) Wavelength-scanned surface-enhanced Raman excitation spectroscopy. *J. Phys. Chem. B* **109**, 11279–11285.

9 Haynes, C. L., McFarland, A. D., Van Duyne, R. P. (2005) Surface-enhanced Raman spectroscopy. *Anal. Chem.* **77**, 338A–346A.

10 Haes, A. J., Van Duyne, R. P. (2004) A unified view of propagating and localized surface plasmon resonance biosensors. *Anal. Bioanal. Chem.* **379**, 920–930.

11 McFarland, A. D., Van Duyne, R. P. (2003) Single silver nanoparticles as real-time optical sensors with zeptomole sensitivity. *Nano Lett.* **3**, 1057–1062.

12 Haes, A. J., McFarland, A. D., Van Duyne, R. P. (2003) Nanoparticle optics: sensing with nanoparticle arrays and single nanoparticles. *Proc. SPIE-Int. Soc. Opt. Eng.* **5223**, 197–207.

13 Yonzon, C. R., Stuart, D. A., Zhang, X., McFarland, A. D., Haynes, C. L., Van Duyne, R. P. (2005) Towards advanced chemical and biological nanosensors – An overview. *Talanta* **67**, 438–448.

14 Haes, A. J., Stuart, D. A., Nie, S. M., Van Duyne, R. P. (2004) Using solution-phase nanoparticles, surface-confined nanoparticle arrays and single nanoparticles as biological sensing platforms. *J. Fluoresc.* **14**, 355–367.

15 Jensen, T. R., Malinsky, M. D., Haynes, C. L., Van Duyne, R. P. (2000) Nanosphere lithography: tunable localized surface plasmon resonance spectra of silver nanoparticles. *J. Phys. Chem. B* **104**, 10549–10556.

16 Jensen, T. R., Duval, M. L., Kelly, L., Lazarides, A., Schatz, G. C., Van Duyne, R. P. (1999) Nanosphere lithography: Effect of the external dielectric medium on the surface plasmon resonance spectrum of a periodic array of silver nanoparticles. *J. Phys. Chem. B* **103**, 9846–9853.

17 Miller, M. M., Lazarides, A. A. (2005) Sensitivity of metal nanoparticle surface plasmon resonance to the dielectric environment. *J. Phys. Chem. B*. **109**, 21556–21565.

18 Xia, Y., Halas, N. J. (2005) Shape-controlled synthesis and surface plasmonic properties of metallic nanostructures. *MRS Bull.* **30**, 338–348.

19 Haynes, C. L., Van Duyne, R. P. (2001) Nanosphere lithography: a versatile nanofabrication tool for studies of size-dependent nanoparticle optics. *J. Phys. Chem. B*. **105**, 5599–5611.

20 Kelly, K. L., Coronado, E., Zhao, L., Schatz, G. C. (2003) The optical properties of metal nanoparticles: the influence of size, shape, and dielectric environment. *J. Phys. Chem. B*. **107**, 668–677.

21 Link, S., El-Sayed, M. A. (1999) Spectral properties and relaxation dynamics of surface plasmon electronic oscillations in gold and silver nano-dots and nano-rods. *J. Phys. Chem. B*. **103**, 8410–8426.

22 Haes, A. J., Van Duyne, R. P. (2002) A nanoscale optical biosensor: sensitivity and selectivity of an approach based on the localized surface plasmon resonance of triangular silver nanoparticles. *J. Am. Chem. Soc.* **124**, 10596–10604.

23 Riboh, J. C., Haes, A. J., McFarland, A. D., Yonzon, C. R., Van Duyne, R. P.

(2003) A nanoscale optical biosensor: Real-time immunoassay in physiological buffer enabled by improved nanoparticle adhesion. *J. Phys. Chem. B* **107**, 1772–1780.

24 Haes, A. J., Zou, S., Schatz, G. C., Van Duyne, R. P. (2004) A nanoscale optical biosensor: the long range distance dependence of the localized surface plasmon resonance of noble metal nanoparticles. *J. Phys. Chem. B.* **108**, 109–116.

25 Haes, A. J., Zou, S., Schatz, G. C., Van Duyne, R. P. (2004) A nanoscale optical biosensor: the short range distance dependence of the localized surface plasmon resonance of silver and gold nanoparticles. *J. Phys. Chem. B.* **108**, 6961–6968.

26 Haes, A. J., Hall, W. P., Chang, L., Klein, W. L., Van Duyne, R. P. (2004) A localized surface plasmon resonance biosensor: First steps toward an assay for Alzheimer's disease. *Nano Lett.* **4**, 1029–1034.

27 Haes, A. J., Chang, L., Klein, W. L., Van Duyne, R. P. (2005) Detection of a biomarker for Alzheimer's disease from synthetic and clinical samples using a nanoscale optical biosensor. *J. Am. Chem. Soc.* **127**, 2264–2271.

28 Yonzon, C. R., Jeoung, E., Zou, S., Schatz, G. C., Mrksich, M., Van Duyne, R. P. (2004) A comparative analysis of localized and propagating surface plasmon resonance sensors: the binding of concanavalin A to a monosaccharide functionalized self-assembled monolayer. *J. Am. Chem. Soc.* **126**, 12669–12676.

29 Zeman, E. J., Schatz, G. C. (1987) An accurate electromagnetic theory study of surface enhancement factors for silver, gold, copper, lithium, sodium, aluminum, gallium, indium, zinc, and cadmium. *J. Phys. Chem.* **91**, 634–643.

30 Athawale, A. A., Katre, P. P., Majumdar, M. B. (2005) Nonaqueous phase synthesis of copper nanoparticles. *J. Nanosci. Nanotechnol.* **5**, 991–993.

31 Malinsky, M. D., Kelly, K. L., Schatz, G. C., Van Duyne, R. P. (2001) Chain length dependence and sensing capabilities of the localized surface plasmon resonance of silver nanoparticles chemically modified with alkanethiol self-assembled monolayers. *J. Am. Chem. Soc.* **123**, 1471–1482.

32 Malinsky, M. D., Kelly, K. L., Schatz, G. C., Van Duyne, R. P. (2001) Nanosphere lithography: effect of substrate on the localized surface plasmon resonance spectrum of silver nanoparticles. *J. Phys. Chem. B* **105**, 2342–2350.

33 El-Sayed, M. A. (2001) Some interesting properties of metals confined in time and nanometer space of different shapes. *Acc. Chem. Res.* **34**, 257–264.

34 Mie, G. (1908) Contributions to the optics of turbid media, especially colloidal metal solutions. *Annalen der Physik (Weinheim, Germany)* **25**, 377–445.

35 Draine, B. T., Flatau, P. J. (1994) Discrete-dipole approximation for scattering calculations. *J. Opt. Soc. Am. A* **11**, 1491–1499.

36 Jensen, T. R., Kelly, K. L., Lazarides, A., Schatz, G. C. (1999) Electrodynamics of noble metal nanoparticles and nanoparticle clusters. *J. Cluster Sci.* **10**, 295–317.

37 Lee, P. C., Meisel, D. (1982) Adsorption and surface-enhanced Raman of dyes on silver and gold sols. *J. Phys. Chem.* **86**, 3391–3395.

38 Sun, Y., Xia, Y. (2002) Shape-controlled synthesis of gold and silver nanoparticles. *Science* **298**, 2176–2179.

39 Jin, R., Cao, Y. C., Hao, E., Metraux, G. S., Schatz, G. C., Mirkin, C. A. (2003) Controlling anisotropic nanoparticle growth through plasmon excitation. *Nature* **425**, 487–490.

40 Daniel, M.-C., Astruc, D. (2004) Gold nanoparticles: assembly, supramolecular chemistry, quantum-size-related properties, and applications toward biology, catalysis, and nanotechnology. *Chem. Rev.* **104**, 293–346.

41 Jin, R., Cao, Y., Mirkin, C. A., Kelly, K. L., Schatz, G. C., Zheng, J. G.

(2001) Photoinduced conversion of silver nanospheres to nanoprisms. *Science* **294**, 1901–1903.

42 Jun, Y.-W., Choi, J.-S., Cheon, J. (2006) Shape control of semiconductor and metal oxide nanocrystals through nonhydrolytic colloidal routes. *Angew. Chem. Int. Ed.* **45**, 3414–3439.

43 Xu, Q., Bao, J., Capasso, F., Whitesides, G. M. (2006) Surface plasmon resonances of free-standing gold nanowires fabricated by nanoskiving. *Angew. Chem. Int. Ed.* **45**, 3631–3635.

44 Haynes, C. L., McFarland, A. D., Zhao, L., Van Duyne, R. P., Schatz, G. C., Gunnarsson, L., Prikulis, J., Kasemo, B., Kaell, M. (2003) Nanoparticle optics: the importance of radiative dipole coupling in two-dimensional nanoparticle arrays. *J. Phys. Chem. B.* **107**, 7337–7342.

45 Jung, L. S., Campbell, C. T., Chinowsky, T. M., Mar, M. N., Yee, S. S. (1998) Quantitative interpretation of the response of surface plasmon resonance sensors to adsorbed films. *Langmuir* **14**, 5636–5648.

46 Sherry, L. J., Chang, S.-H., Schatz, G. C., Van Duyne, R. P., Wiley, B. J., Xia, Y. (2005) Localized surface plasmon resonance spectroscopy of single silver nanocubes. *Nano Lett.* **5**, 2034–2038.

47 Zhang, X., Hicks, E. M., Zhao, J., Schatz, G. C., Van Duyne, R. P. (2005) Electrochemical tuning of silver nanoparticles fabricated by nanosphere lithography. *Nano Lett.* **5**, 1503–1507.

48 Whitney, A. V., Elam, J. W., Zou, S., Zinovev, A. V., Stair, P. C., Schatz, G. C., Van Duyne, R. P. (2005) Localized surface plasmon resonance nanosensor: a high-resolution distance-dependence study using atomic layer deposition. *J. Phys. Chem. B.* **109**, 20522–20528.

49 Hicks, E. M., Zou, S., Schatz, G. C., Spears, K. G., Van Duyne, R. P., Gunnarsson, L., Rindzevicius, T., Kasemo, B., Kaell, M. (2005) Controlling plasmon line shapes through diffractive coupling in linear arrays of cylindrical nanoparticles fabricated by electron beam lithography. *Nano Lett.* **5**, 1065–1070.

50 Kwak, E., Henzie, J., Chang, S., Gray, S. K., Schatz, G. C., Odom, T. W. (2005) Surface plasmon standing waves in large-area subwavelength hole arrays. *Nano Lett.* **5**, 1963–1967.

51 Brolo, A. G., Gordon, R., Leathem, B., Kavanagh, K. L. (2004) Surface plasmon sensor based on the enhanced light transmission through arrays of nanoholes in gold films. *Langmuir* **20**, 4813–4815.

52 Ebbesen, T. W., Lezec, H. J., Ghaemi, H. F., Thio, T., Wolff, P. A. (1998) Extraordinary optical transmission through sub-wavelength hole arrays. *Nature* **391**, 667–669.

53 Hicks, E. M., Zhang, X. Y., Zou, S. L., Lyandres, O., Spears, K. G., Schatz, G. C., Van Duyne, R. P. (2005) Plasmonic properties of film over nanowell surface fabricated by nanosphere lithography. *J. Phys. Chem. B* **109**, 22351–22358.

54 Haes, A. J., Zhao, J., Zou, S., Own, C. S., Marks, L. D., Schatz, G. C., Van Duyne, R. P. (2005) Solution-phase, triangular Ag nanotriangles fabricated by nanosphere lithography. *J. Phys. Chem. B* **109**, 11158–11162.

55 Wiley, B., Sun, Y., Mayers, B., Xia, Y. (2005) Shape-controlled synthesis of metal nanostructures: The case of silver. *Chemistry – A European Journal* **11**, 454–463.

56 Im Sang, H., Lee Yun, T., Wiley, B., Xia, Y. (2005) Large-scale synthesis of silver nanocubes: the role of HCl in promoting cube perfection and monodispersity. *Angew. Chem. Int. Ed. Engl.* **44**, 2154–2157.

57 Englebienne, P. (1998) Use of colloidal gold surface plasmon resonance peak shift to infer affinity constants from the interactions between protein antigens and antibodies specific for single or multiple epitopes. *Analyst* **123**, 1599–1603.

58 Raschke, G., Kowarik, S., Franzl, T., Soennichsen, C., Klar, T. A., Feldmann, J., Nichtl, A., Kuerzinger, K. (2003) Biomolecular recognition based on single gold nanoparticle light scattering. *Nano Lett.* **3**, 935–938.

59 Gong, Y., Chang, L., Viola, K. L., Lacor, P. N., Lambert, M. P., Finch, C. E., Krafft, G. A., Klein, W. L. (2003) Alzheimer's disease-affected brain: Presence of oligomeric Ab ligands (ADDLs) suggests a molecular basis for reversible memory loss. *Proc. Natl. Acad. Sci. USA* **100**, 10417–10422.

60 Lambert, M. P., Barlow, A. K., Chromy, B. A., Edwards, C., Freed, R., Liosatos, M., Morgan, T. E., Rozovsky, I., Trommer, B., Viola, K. L., et al. (1998) Diffusible, nonfibrillar ligands derived from Abeta1-42 are potent central nervous system neurotoxins. *Proc. Natl. Acad. Sci. USA* **95**, 6448–6453.

61 Wang, H.-W., Pasternak, J. F., Kuo, H., Ristic, H., Lambert, M. P., Chromy, B., Viola, K. L., Klein, W. L., Stine, W. B., Krafft, G. A., et al. (2002) Soluble oligomers of b-amyloid (1-42) inhibit long-term potentiation but not long-term depression in rat dentate gyrus. *Brain Res.* **924**, 133–140.

62 Walsh, D. M., Selkoe, D. J. (2004) Oligomers in the brain: The emerging role of soluble protein aggregates in neurodegeneration. *Protein Peptide Lett.* **11**, 213–228.

63 Lambert, M. P., Viola, K. L., Chromy, B. A., Chang, L., Morgan, T. E., Yu, J., Venton, D. L., Krafft, G. A., Finch, C. E., Klein, W. L. (2001) Vaccination with soluble A oligomers generates toxicity-neutralizing antibodies. *J. Neurochem.* **79**, 595–605.